ENGINEERING Environment
2026, 20(3): 34 https://doi.org/10.1007/s11783-026-2134-8

RESEARCH ARTICLE

Combined electric field treatment with copper and silver for water disinfection

Mourin Jarin[1], Xing Xie ✉ [1,2]

1. School of Civil and Environmental Engineering, Georgia Institute of Technology, Atlanta, GA 30332, USA
2. Institute for Matter and Systems, Georgia Institute of Technology, Atlanta, GA 30332, USA

HIGHLIGHTS

- A lab-on-a-chip is used to observe the inactivation of *Staphylococcus epidermidis*.
- The synergistic effects of electric field treatment with Cu and Ag are quantified.
- The highest synergy is observed using EFT combined with Cu and Ag.
- 95% inactivation was achieved using only 34 kV/cm, 200 µg/L Cu, and 10 µg/L Ag.

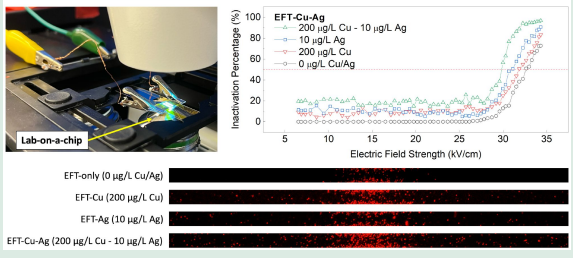

ABSTRACT: Domestic water is of great importance to our modern lives and yet opportunistic pathogens like *Legionella*, *Cryptosporidium*, and *Giardia* are the largest cause of outbreaks and illnesses in our potable water supply. Previously, electric field treatment (EFT) in combination with copper (Cu) was studied at the microscale and found to have synergistic performance enhancing the inactivation of bacteria. In this study, a lab-on-a-chip device is used to better understand, observe, and quantify the synergistic effect when combining EFT with Cu and Ag for water disinfection. *Staphylococcus epidermidis* is studied as a model bacterium. Using Cu and/or Ag ions with various concentrations as the chemical disinfection agents and EFT as the physical disinfection aid, we can ultimately reduce the metal ion concentration and energy required to achieve effective inactivation of bacteria. In this study, the highest synergies were measured using EFT with Cu and Ag together, for example, achieving > 95 % inactivation using only 34 kV/cm electric field strength, 200 µg/L Cu, and 10 µg/L Ag. These results can be used to optimize and customize the disinfection performance of EFT devices to adapt for its various point-of-use applications.

KEYWORDS: Copper/silver, Electric field treatment, Electroporation, Bacteria inactivation, LOAC

1 Introduction

Domestic water systems are of great importance to our daily lives and yet opportunistic pathogens like *Legionella*, *Cryptosporidium*, and *Giardia* are the largest cause of outbreaks and illnesses in our potable water demonstrating their continued threat (Benedict et al., 2017). Out of these chlorine-resistant pathogens of concern, the most commonly reported source of infections stems from *Legionella* outbreaks with many exposures linked to the water systems of hotels, large

✉ Corresponding author. E-mail: xing.xie@ce.gatech.edu
Article history: Received 9 May 2025, Revised 16 October 2025, Accepted 17 October 2025, Available online 1 January 2026

venues, and hospital buildings (Berthelot et al., 1998; Ricketts and Joseph, 2005; Mouchtouri et al., 2007). Because Legionnaires' disease is most threatening when aerosolized from contaminated water, outbreaks typically occur from the potable water in large buildings, cooling towers, pools and spas, decorative fountains, and industrial waters (Van Heijnsbergen et al., 2015; Garrison et al., 2016). Large and complex buildings are responsible for 90% of legionellosis cases, mostly found in the plumbing distribution systems (June and Dziewulski, 2018; Carlson et al., 2020). Important to note, the occurrence of these chlorine-resistant pathogen outbreaks has increased by over 500% since 2000 and *Legionella* is currently the most reported cause of all outbreak-associated deaths in the USA (Benedict et al., 2017; CDC, 2018). Despite the many outbreaks, the USEPA has not set strict guidelines on monitoring and controlling chlorine resistant pathogens in our water stream. The USEPA specifies a detectable residual disinfectant (*i.e.*, a residual concentration of chlorine) as enough to provide a preventative treatment measure for opportunistic pathogens, resulting in any active monitoring or detection as not required and unenforced (USEPA, 1989; LeChevallier, 2019).

The USEPA currently cites 6 different methods used to mitigate pathogens like *Legionella* that include chlorine, chlorine dioxide, monochloramine, ozone, ultraviolet (UV) disinfection, and copper-silver ionization (CSI), while noting these methods can range in their effectiveness and potential negative externalities with use (USEPA, 2024c). The most commonly used chlorine solutions (including free chlorine, chlorine dioxide, monochloramine) are currently disadvantaged as they can cause corrosion in the plumbing (USEPA, 2024c). Other concerns for chlorine based disinfection result from the formation of carcinogenic disinfection by-products (DBPs) well established in the literature (USEPA, 2024b). Ozonation is also capable of resulting DBPs, but unlike chlorine based solutions, is short lived and does not offer any residual disinfectant (Carlson et al., 2020; USEPA, 2024c). UV disinfection is only active in the exposed regions of flow, providing no residual disinfection and comes with the risk of mercury contamination if the lamps were to lose integrity and break over time, although does not produce any harmful DBPs like the more widely used solutions (USEPA, 2006, 2024c; Wright et al., 2012).

Lastly, CSI has been commercially available for several years now as a popular method in controlling *Legionella* in large plumbing systems as a supplemental decentralized treatment (June and Dziewulski, 2018). Typically copper (Cu) and silver (Ag) ions are released into the hot water stream using a direct current applied to sacrificial electrodes in a flow cell (Dziewulski et al., 2015). There are also many studies that speak to the synergy between antimicrobial metals alone, the most well-known being Cu and Ag as used currently for CSI applications (Garza-Cervantes et al., 2017; Raja et al., 2023; Soliman et al., 2023; Vasiliev et al., 2023). Although CSI is naturally biocidal at high concentrations, the main setbacks are that it can result adverse health effects if ingested at toxic concentrations and can also cause the potable water to taste and look unappealing (Rohr et al., 1999; Araya et al., 2004). When antimicrobial metals are used independently to treat drinking water, high concentrations (above the secondary maximum contaminant levels (SMCLs)) may be necessary, resulting in the final treated water to be non-potable for human consumption (Dietrich and Burlingame, 2015; USEPA, 2024a). Specifically for Cu and Ag, the SMCLs are 0.1 and 1.0 mg/L, respectively (Dietrich and Burlingame, 2015; USEPA, 2024a). Because of these reasons, CSI is mainly used to treat domestic hot water and not specifically drinking water alone. In order to use antimicrobial metals for drinking water disinfection, it is necessary to lower the concentration required as this remains a large barrier to wide scale application.

One possible solution to this large barrier could be the use of electric field treatment (EFT) which has been applied for microbial inactivation for over a century (Raso et al., 2022). With the discovery of electroporation, EFT has made significant improvement in both application and understanding of mechanisms in combination with other techniques (Weaver and Chizmadzhev, 1996). During EFT, when the electric field strength surpasses a threshold (~10 kV/cm), the membranes of microorganisms are damaged irreversibly, ultimately causing cell death (Wang et al., 2019). Currently, EFT is mostly applied in liquid food processing for beverages but has potential to be enhanced further for various applications (Milani et al., 2015; Timmermans et al., 2019; Alirezalu et al., 2020). EFT has been studied previously in combination with *in-situ* Cu release and the addition of antimicrobial metal ions to find synergistic performance in inactivation (Zhou et al., 2019).

In our recent work, electric field treatment (EFT) was observed on a lab-on-a-chip (LOAC) device when combined with Cu ions to further enhance the inactivation efficiency of *S. epidermis* (Jarin et al., 2024). Additionally, a synergy between EFT and Cu was observed showing promise for physical disinfection approaches to succeed in combination with

antimicrobial metals. This leads us to believe the addition of EFT could further aid in increasing the inactivation performance of other antimicrobial metals for water disinfection and that the synergy between metals could be enhanced even more with EFT to provide high disinfection performance at lower and safer metal ion concentrations. In this paper, we use a lab-on-a-chip device to study the effects of EFT with Cu and Ag to better understand the synergy between EFT with Cu and Ag for inactivation of *S. epidermis* as the model bacteria. The mechanisms involved for both metals, their synergy with one another, and their combination approaches with EFT are elucidated. Lastly, the limitations of this study, future work, and potential impacts to the field of water disinfection are discussed.

2 Materials and methods

2.1 Fabrication and design of the LOAC

Lab-on-a-chip (LOAC) platforms provide notable benefits over conventional bulk electroporation systems (Boukany et al., 2011). Due to the micro- and nanoscale dimensions of the electrodes, these devices can generate highly concentrated electric fields while operating at substantially lower voltages (Wang et al., 2019). In this study, one key benefit of using LOACs is their ability to facilitate real-time observation and detailed analysis of electric field-induced microbial inactivation at the single-cell level. Compared to larger-scale setups, LOAC systems minimize chemical and material usage, and they reduce both time and spatial demands through more efficient experimental design. For bacterial experiments, more traditional batch scale involves larger volumes and bacteria concentrations, while plate count analysis is required as well. Moreover, such approaches lack the flexibility to explore a spectrum of electric field intensities in a single run or to produce the high-resolution data captured via LOAC-based experiments (Wang et al., 2019, 2022; Wang and Xie, 2023, 2024; Jarin et al., 2024).

The LOAC device used in this study was fabricated following previously reported methods. (Jarin et al., 2024) Briefly, gold electrodes were patterned onto a glass substrate using conventional photolithographic and lift-off techniques. As illustrated in Fig. 1a and labeled in Fig. 1b, the device includes 30 symmetrically curved microchannels arranged in parallel. These curved electrodes were intentionally designed to produce a gradient of electric field strengths along the x-axis. As shown in Fig. 1c, the spatial relationship between the electrode shape and electric field distribution is governed by a curvature model using Eq. (1), where x and w represent half the channel's length and width, w_0 is the center width at $x = 0$ and k is a geometric constant (0.005 μm^{-1}). Each microchannel spans 440 μm in length, narrowing to 20 μm at the midpoint to enhance the field effect. When voltage is applied, the resulting electric field at any point is linearly determined according to Eq. (2), where E is the electric field and U the applied voltage. COMSOL Multiphysics simulations of this geometry under a 70 V input confirmed a peak field strength of approximately 35 kV/cm at the center of each channel.

2.2 Cell preparation and immobilization

To ensure consistent results across all experiments, *Staphylococcus epidermidis* (ATCC, cat# 12228, USA) was immobilized onto the LOAC channel surfaces, specifically in the regions between the curved electrode structures (see Fig. 1b). The preparation and immobilization protocol followed previously established procedures (Jarin et al., 2024). In brief, the chips were pre-treated with a layer of poly-L-lysine (Sigma-Aldrich, cat# A-005-C, USA) to promote adherence of the bacterial cells via electrostatic attraction. For coating, poly-L-lysine was diluted in a 1:1 ratio with 2 mol/L borate buffer—prepared by dissolving 3.1 g of boric acid (Millipore, cat# 100765, USA) and 0.5 g of NaOH (Millipore, cat# SX0593-1, USA)—and applied evenly to each chip. After incubation for approximately 2 h, excess coating solution was removed by rinsing with deionized water. The chips were then dried and heat-treated at 60 °C for 10 min to complete the surface functionalization process. Once dry, the chips were ready for use in bacterial immobilization.

The model bacteria *S. epidermidis* was used to assess the inactivation efficiency of all experiments as it is commonly used in water disinfection, antimicrobial testing, and EFT based research (Helbling and VanBriesen, 2007; Wen et al., 2017; Garner, 2019; Gupta et al., 2022; Jarin et al., 2024). Although not a chlorine-resistant pathogen in the environment, *S. epidermidis* is the most consistent and established model bacteria for the current LOAC experiments. Cultures were grown in nutrient broth (Becton Dickinson, cat# 234000, USA) at 35 °C for approximately 15 h under standard incubation conditions. To prepare the cells for loading onto the device, 1 mL of the bacterial suspension was centrifuged at 1000 g for 5 min, then resuspended in 10 mmol/L phosphate buffer (pH 8.5). This wash cycle was repeated three times to ensure cleanliness and consistency. Approximately

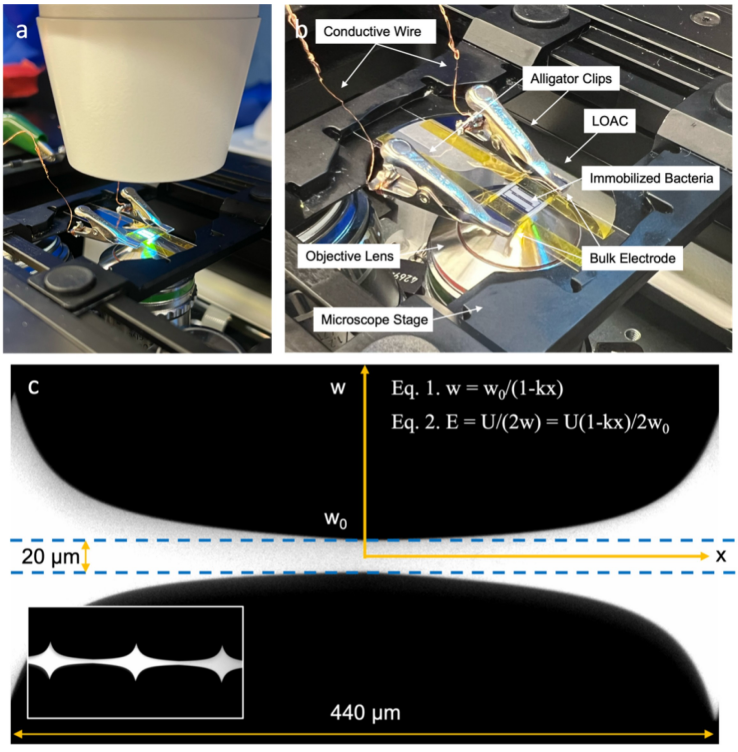

Fig. 1 Operational view of the lab-on-a-chip (LOAC) system. (a) Image showing the LOAC system actively mounted on a fluorescence microscope during use. (b) A magnified view highlighting the device's placement on the microscope objective, with labeled components relevant for microscale observation. (c) A microscope image of an individual microchannel from the chip. The curved electrode geometry is shown, with associated design parameters w, w_0, and x, as referenced in Eqs. (1) and (2). The blue dashed rectangle indicates the standardized region used for experimental data collection. The inset in the lower-left corner provides a wider view, displaying multiple adjacent channels for spatial context. For color figure references, please consult the online version of this article.

50–100 μL of the final bacterial suspension was applied to each chip and allowed to incubate undisturbed for 50 min, promoting effective immobilization. Excess liquid and unattached cells were gently removed with deionized water. All LOAC devices in this study were prepared using this consistent bacterial loading protocol.

2.3 Antimicrobial metals preparation

For all experiments involving metal ion treatments, copper and silver were tested independently and in combination across multiple concentrations. Copper nitrate trihydrate (Sigma-Aldrich, CAS# 10031-43-3, USA) and silver nitrate (Sigma-Aldrich, CAS# 7761-88-8, USA) were selected to ensure consistency in anionic composition, thereby minimizing the potential for precipitate formation when both metals were used simultaneously. Each salt was dissolved in deionized water, and sodium nitrate (VWR, cat# 0598, USA) was added to precisely control solution conductivity. To maintain consistency across all trials, the conductivity was adjusted to 10 ± 2 μS/cm, as measured using an Orion Versa Star Pro conductivity probe (Thermo Scientific, USA) (Wang et al., 2019). All concentrations of metals tested on the LOAC were kept at concentrations below the SMCL limits, specifically, Ag ranged between 0–0.1 mg/L and Cu between 0–0.8 mg/L (Dietrich and Burlingame, 2015; USEPA, 2024a). For control experiments with no EFT applications and one metal tested at a time, ~100 μL of each metal solution at varying concentrations was applied to the top of the chip and a 2-h residual effective treatment time was completed before dye staining and imaging. While it can be argued EFT-Ag and EFT-Cu can not be compared due to the concentration differences of the metal ions, we believe that the synergy between EFT and different antimicrobial metals can not be observed or compared at all without using the metals within their respective toxicity ranges for this specific study. For experiments with combined Cu and Ag, a combined solution was made accordingly with the respective metal ion concentrations while maintaining the conductivity between 10 ± 2 μS/cm for experiments

using EFT and were then used similarly with ~100 μL aliquots and a wait time of 2 h.

2.4 Electric field treatment

In all EFT-based experiments, electric pulses were applied under standardized conditions to maintain consistency across trials. The operating parameters included a 70 V square-wave voltage, 500 ns pulse width, and a 500 μs period, resulting in a duty cycle of 0.1%. These values were selected based on prior optimization studies and previously published protocols (Jarin et al., 2024). The total effective exposure time, calculated as the product of pulse width and number of pulses, was maintained at 20 ms. To focus exclusively on evaluating the interaction between EFT and antimicrobial metal ions, only a single set of pulsed electric field parameters was used throughout this study, in line with previous recommendations that have characterized varying EFT conditions in detail (Wang et al., 2019). Electric pulses were delivered using an Avtech AV-1010-B high-speed pulse generator, controlled by a waveform generator (Keysight 33509B, USA). Following electric field exposure and/or metal ion treatment, each sample underwent a 2-h post-treatment period prior to fluorescent staining and microscopy, ensuring results captured the representative inactivation behavior at this microscale.

To ensure that the observed microbial inactivation was attributed solely to electric field treatment (EFT) and the antimicrobial activity of metal ions, each experiment was carefully designed to prevent the formation of reactive oxygen species (ROS), bubble generation, or significant thermal effects. Prior validation confirmed that the selected operating conditions minimized these secondary phenomena (Jarin et al., 2024). In particular, maintaining a low duty cycle of 0.1% was critical for this control, as the extended rest intervals between pulses—three orders of magnitude longer than each pulse—help dissipate any localized heat and prevent excessive energy buildup (Wang and Xie, 2024). This configuration effectively limited unintended side effects, allowing us to isolate and assess the specific contributions of EFT, copper, and silver treatments. These preventative measures support the reliability of our conclusions regarding the synergistic and independent disinfection roles of EFT and antimicrobial metals.

2.5 Microscope image processing

Following the 2-h post-treatment incubation period, all chips were mounted onto cover glasses for fluorescence imaging (see Figs. 1a and 1b). A single-stain fluorescent labeling approach was employed using propidium iodide (PI), a dye widely recognized for indicating membrane damage in microbial cells. PI selectively penetrates cells with compromised membranes and binds to intracellular DNA, producing a measurable fluorescent signal. This method has been extensively used in prior studies examining membrane permeability and electroporation-based inactivation (Arndt-Jovin and Jovin, 1989; Li and Lin, 2011; Garner, 2019). Although reversible electroporation could, in theory, impact the interpretation of viability, earlier research has shown negligible differences in staining outcomes regardless of whether PI is applied before or after treatment (Jarin et al., 2024). Given the 2-h delay between treatment and staining, we interpret PI-positive cells in this study as nonviable. This methodological note is included here to provide transparency regarding possible sources of uncertainty, ensuring a clear understanding of how disinfection efficacy was assessed in our EFT-Cu and EFT-Ag experiments.

Microscopic imaging was conducted using a Zeiss Axio Observer 7 inverted fluorescence microscope equipped with differential interference contrast (DIC) and fluorescent channels, and images were captured via a CCD camera. Image processing and quantification of bacterial inactivation were performed using MATLAB (version 2023a, MathWorks). For each LOAC device, up to 30 repeat channels were analyzed, and data were aggregated from all usable channels to compute inactivation percentages along the x-axis. Data analysis focused on the blue-highlighted region shown in Fig. 1c, where custom MATLAB scripts were used to isolate, align, and segment the selected area for every image collected. Each image segment was divided into 120 vertical sections, with binarization applied to differentiate between total and fluorescent (*i.e.*, PI-stained) cells. Inactivation efficiency was computed as the ratio of stained to total cells in each section. Due to the symmetry of the channel design, this approach yielded 60 unique measurement points per channel, effectively doubling to 120 data points with mirrored duplicates. Final results are presented as the mean of these values across all valid replicate channels, with error bars indicating 95% confidence intervals. This image analysis framework was previously developed to provide consistent, high-throughput quantification across a range of LOAC-based disinfection studies, including this work involving EFT and metal ions. Further implementation details can be found in our earlier publication (Jarin et al., 2024).

2.6 Data analysis

For the rest of the data analysis, Microsoft Excel was used to calculate the synergy values via Bliss Independence Model (BIM), p-values to assess significance via two-tailed t-tests, and significance via analysis of variance (ANOVA) for some cases (Hegreness et al., 2008; Garza-Cervantes et al., 2017). The BIM allows us to calculate the significance of any synergy present between each combination case of experiments using Eq. (3) (below). All inputted values are calculated as the percent of bacteria that survived the treatment out of the maximum capacity of 100% (For example, if 70% of bacteria are inactivated, then 30% are considered to be alive and used for the representative value in the calculation). Using the BIM calculation, a synergy (S) value is resulted where S > 0 indicates a present synergy, S = 0 indicates an additive result, and S < 0 indicates an antagonistic result.

$$S = \left(\frac{f_{x0}}{f_{00}}\right)\left(\frac{f_{0y}}{f_{00}}\right) - \frac{f_{xy}}{f_{00}}, \quad (3)$$

where the S value indicates the difference between the predicted value of the individual components (x, y) and the combined result (xy), f_{x0} refers to the survival percentage of one tested condition, f_{0y} refers to another tested condition, f_{00} refers to the control case for any given experiment, and f_{xy} refers to the combined approaches of f_{x0} and f_{0y}. Examples of how the equation was adjusted for each experimental case is also listed for the reader's understanding and clarification.

For example, when testing the combination of Cu and Ag only, we use Eq. (4).

$$S = \left(\frac{f_{\mathrm{Cu}}}{f_{\mathrm{Control}}}\right)\left(\frac{f_{\mathrm{Ag}}}{f_{\mathrm{Control}}}\right) - \frac{f_{\mathrm{Cu-Ag}}}{f_{\mathrm{Control}}}, \quad (4)$$

where f_{Cu} refers to conditions with Cu present, f_{Ag} refers to conditions with Ag present, f_{Control} refers to the control case (conditions where no antimicrobial metals are present), and $f_{\mathrm{Cu\text{-}Ag}}$ refers to the combined approach using Cu and Ag.

When testing the combination of EFT and Cu, we use Eq. (5).

$$S = \left(\frac{f_{\mathrm{EFT-only}}}{f_{\mathrm{Control}}}\right)\left(\frac{f_{\mathrm{Cu}}}{f_{\mathrm{Control}}}\right) - \frac{f_{\mathrm{EFT-Cu}}}{f_{\mathrm{Control}}}, \quad (5)$$

where $f_{\mathrm{EFT\text{-}only}}$ refers to the EFT-only condition (with no antimicrobial metals) and f_{Cu} refers to conditions with Cu present. Also, f_{Control} refers to the control case (conditions where no antimicrobial metals or EFT are present), and $f_{\mathrm{EFT\text{-}Cu}}$ refers to the combined approach using EFT-Cu.

When testing the combination of EFT, Cu, and Ag, we use Eq. (6).

$$S = \left(\frac{f_{\mathrm{EFT-only}}}{f_{\mathrm{Control}}}\right)\left(\frac{f_{\mathrm{Cu-Ag}}}{f_{\mathrm{Control}}}\right) - \frac{f_{\mathrm{EFT-Cu-Ag}}}{f_{\mathrm{Control}}}, \quad (6)$$

where $f_{\mathrm{EFT\text{-}only}}$ refers to the EFT-only condition (without antimicrobial metals) and $f_{\mathrm{Cu\text{-}Ag}}$ refers to combined approaches using Cu-Ag without EFT. Lastly, $f_{\mathrm{EFT\text{-}Cu\text{-}Ag}}$ refers to the combined approach using EFT with Cu and Ag.

3 Results

3.1 Inherent antimicrobial properties of Cu and Ag ions

Both Cu and Ag were tested in varying concentrations individually to determine the inactivation capability when using the LOAC device. This was necessary to gain understanding of the control values and ensure we can capture accurate and consistent cell death with each of the metals on the device before attempting to add other conditions to understand the synergy. Figure 2 shows the results for inactivation percentage on the LOAC over varying concentrations individually. The results for both metals show an increase with increasing concentration. For Cu, ~10% cell inactivation was observed when adding 200 μg/L and this increased to ~23% with 800 μg/L (Fig. 2a). For Ag, ~7% cell inactivation was observed when adding 10 μg/L and this increased to ~51% with 100 μg/L (Fig. 2b). These results show the successful observation and quantification of each antimicrobial metal and its respective cell death using the LOAC device. Since all the concentrations for Cu and Ag are in ranges within the SMCLs for the USEPA secondary drinking water guidelines (Cu 1.0 mg/L and Ag 0.1 mg/L), it is also expected that we see different ranges in toxicity for each. (USEPA, 2024a) As predicted, Ag has a lower SMCL and is more toxic, requiring lower concentrations to cause cell death.

The results in Fig. 2b are not surprising as Ag is well known to be very toxic to bacteria due to its biocidal properties, working well at extremely low concentrations (Lemire et al., 2013). Although there are many mechanisms proposed for how different antimicrobial metals may inactivate bacteria, Ag in particular is heavily evidenced to severely compromise the integrity of the cytoplasmic membrane, impair the membrane function through loss of membrane potential, disrupt the bacterial electron transport chain, and engage in some *in vivo* protein dysfunction and thiol depletion (Bragg and Rainnie, 1974; Feng et al., 2000; Dibrov

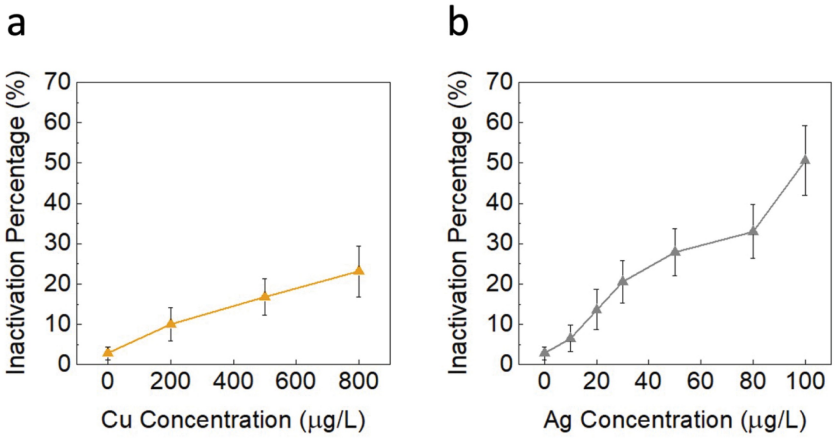

Fig. 2 Inactivation efficiency of Cu (a) and Ag (b) applied individually on the LOAC. The *y*-axis represents inactivation percentage, and the *x*-axis is the varying concentrations for each antimicrobial metal ion. There is no EFT applied in these three cases. Higher concentrations of Cu were not tested in this study as concentrations beyond Cu's MCL were realized in our previous work(Jarin et al., 2024). Error bars represent 95% confidence intervals of the mean values for up to 30 replicate channels.

et al., 2002; Gordon et al., 2010; Li et al., 2010; Lemire et al., 2013; Alherek and Basu, 2023). Studies have also observed Ag ions to potentially penetrate bacteria and turn their DNA into a condensed form, blocking DNA replication, and leading to an eventual destruction of the cell (Marambio-Jones and Hoek, 2010). Further detailed examples of relevant mechanism studies are discussed in the Supplymentary Materials.

Cu is well known for its biocidal properties in bacteria as well, specifically its abilities to engage in protein dysfunction, impair the membrane function through membrane damage or increased permeability, and production of intracellular reactive oxygen species (ROS) and antioxidant depletion (Valko et al., 2005; Macomber et al., 2007; Warnes and Keevil, 2011; Warnes et al., 2012; Lemire et al., 2013; Alherek and Basu, 2023; Jarin et al., 2024). Many studies support Cu's ability to generate ROS by reduction through a Fenton-like reaction, leading to enzyme/non-enzyme mediated oxidative damage with lipid peroxidation, protein oxidation, and even DNA damage (Ray et al., 2012; Pham et al., 2013; Yang et al., 2014; Salah et al., 2021). Additionally, several authors have studied Cu ions and their successful ability to damage the membrane, infiltrate the cell, and induce oxidative stress via endogenous ROS (Prabhu et al., 2010; Grass et al., 2011; Ray et al., 2012; Salah et al., 2021). Despite the many different ways these two metals can cause inactivation of bacteria, many of the attack pathways overlap, leading us to believe further study of the potential synergies between them may be promising as well.

3.2 Synergy between Cu and Ag without EFT

While the synergy between Cu and Ag has been well studied in the literature, this is the first that it has been studied on immobilized bacteria using a LOAC. The results are shown in Fig. 3 for bacteria inactivation using Cu and Ag on the LOAC device with no EFT. The red dots indicate fluorescence of the PI dye and in this work, we refer to this as inactivated cells (please see methods section for further details). The control images and values for inactivation are presented in each square along with the error. There is clearly increased fluorescence (more red cells) as we increase the concentration of each metal present. Looking at the inactivation values, when the concentrations of either or both metals increase, the inactivation efficiency also increases in both cases as expected. Although the inactivation values increasing in comparison to their individual control experiments is promising, it does not signify any synergy presence between the metals.

Figure 4a displays the correlating heatmaps for the theoretical additive of each combination of concentration case if no synergy was present (expecting the resulting inactivation of any combination to be relatively close to each metal's previous inactivation value added together). In Fig. 4b, the actual inactivation results are shown in heatmap form. The change in the intensity of the colors displays where there is an increase in actual cell death in comparison to the theoretical additive plot. In this case, we see insignificant and dramatic changes of color, and increased inactivation compared to the additive values. There is clearly more intensified color present when the

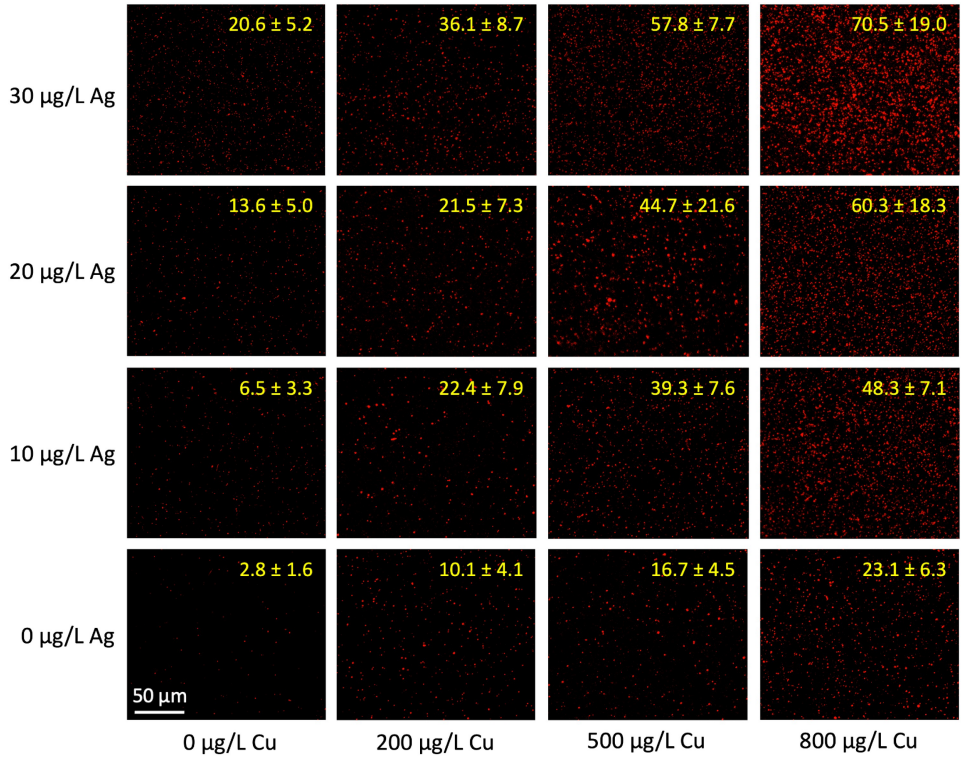

Fig. 3 Fluorescence microscope images of Cu and Ag for individual and combination cases on the LOAC device. The red dots indicate inactivated cells here while the analyzed and calculated inactivation percentage and error is highlighted in the corners of each image. The errors here refer to the 95% confidence intervals of the mean values. For color figure references, please consult the online version of this article.

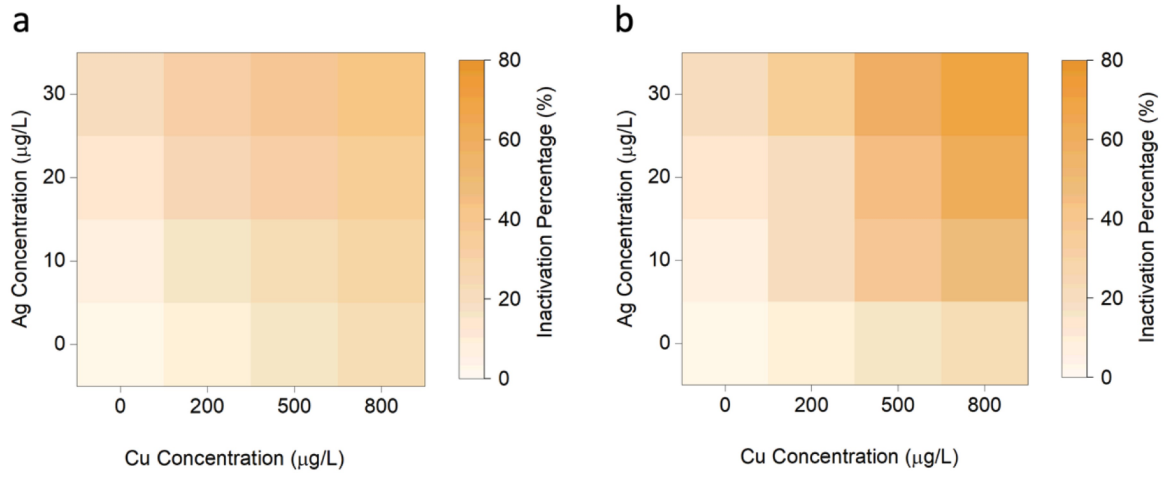

Fig. 4 Inactivation efficiency heatmaps for the theoretical additive (a) and measured results (b) for Cu and Ag on the LOAC. The color scale indicates the level of inactivation achieved for each case. The theoretical additive values (a) are calculated by adding each respective Cu control value with the respective Ag control value within the matrix to approximate the inactivation of each combination case assuming no presence of synergy. For color figure references, please consult the online version of this article.

concentration increases, indicating some synergy may be present in these conditions. All nine experimental cases exhibited statistically significant differences when compared to their theoretical additive conditions ($p < 0.01$).

Figure 5 displays the Bliss Independence Model

(BIM) heatmap for Cu and Ag. There are many positive S values indicating significant synergy between Cu and Ag, specifically increasing as the concentrations for both ions increase. One near zero value is observed (in white), which we consider to be additive inactivation. No negative values were observed. Cu and Ag showed strong positive inactivation synergy present in majority of the tested combinations, specifically highest at 0.34 for 800 μg/L Cu and 30 μg/L Ag. This is not surprising as there is ample literature and historical knowledge supporting the discussion of Cu and Ag's synergistic behaviors when used together (as previously discussed).

The combination of these two antimicrobial metals may reduce the time required to achieve complete inactivation which may also contribute to the increased inactivation efficiency observed in most cases (Raja et al., 2023). Specifically considering the overlapping biocidal mechanisms of Cu and Ag individually, it is highly likely that the mechanisms in the combination experiments involve some initial increase in the membrane permeability and/or direct damage to the membrane/cell wall, followed by disruption of various intracellular components and processes (Garza-Cervantes et al., 2017). Previous studies have concluded that *E. coli* and *B. subtilis* tested with Cu and Ag exhibited synergistic effects mainly through an increased cell permeability (Garza-Cervantes et al., 2017). Additionally, other research done on *E. coli* and *P. aeruginosa* suggests that the synergistic effect of Cu and Ag is dependent on Ag damaging the outer membranes of the bacteria while Cu acts on the other cell structures as it may be slower to cause outer membrane destruction (Vasiliev et al., 2023). As Cu and Ag have somewhat similar attack pathways for inactivating bacteria, their teamwork in combination here to take advantage of their stronger abilities may result in the increased S values we see.

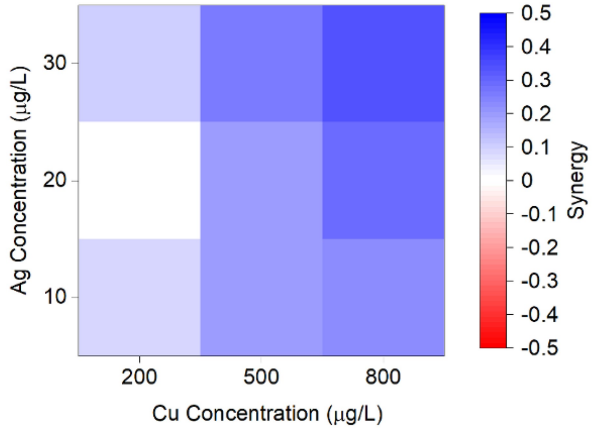

Fig. 5 Synergy (S) values determined via Bliss Independence Model for the combinations of Cu and Ag on the LOAC. For color figure references, please consult the online version of this article.

3.3 Inactivation efficiency of Cu or Ag with EFT

Understanding the inactivation mechanisms of both Cu and Ag, and their promising potential to formulate additional synergies with EFT, like Cu has done in previous works, here we show the results when combined individually with EFT in Fig. 6. In this figure, the inactivation efficiency is fairly stable until a certain electric field strength is reached. This indicates the threshold of EFT required to initiate electroporating bacteria regardless of the additional metal ions present. After the threshold is crossed, we see the swift incline of inactivation percentage where the bacteria are now much more sensitive to the variations in electric field strength. For all experiments for each of the two metals

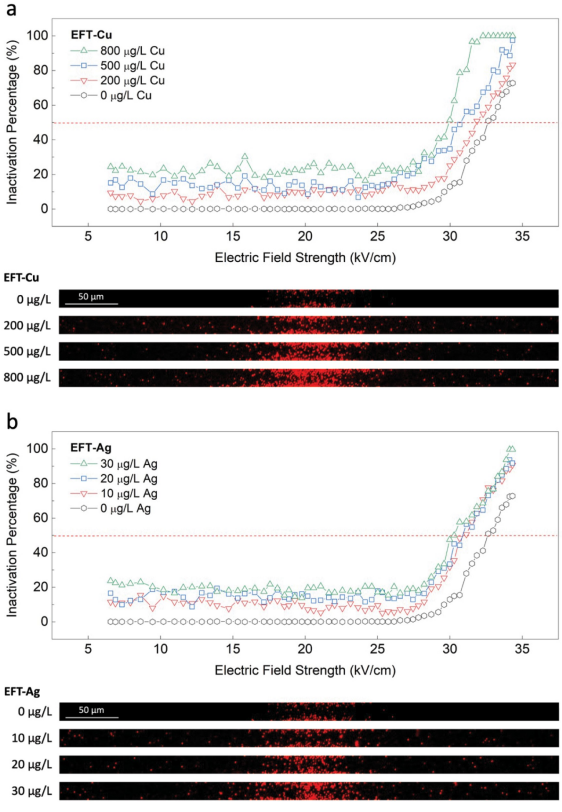

Fig. 6 Inactivation efficiency and representative fluorescence microscopy images for EFT-Cu (a) and EFT-Ag (b) across a range of metal concentrations and electric field strengths. A red dashed line indicates the lethal electroporation threshold (LET), defined as the point where bacterial inactivation reaches 50%. Red fluorescent dots mark the positions of inactivated cells on the LOAC surface. Error bars corresponding to 95% confidence intervals are provided in Supplementary Figs. S1 and S2. For color-related figure elements, please refer to the online version of this article.

(EFT-Cu and EFT-Ag), statistically significant differences were exhibited when compared to the EFT-only control with no antimicrobial metals present ($p<0.001$). Figure 6a shows the inactivation percentage of EFT-Cu where the inactivation efficiency increases for increasing Cu concentration and increased electric field strengths. The inactivation efficiency quickly spikes to 100% for the 800 μg/L Cu case at only 32 kV/cm, while without any Cu, the EFT-only reaches a mere 41% inactivation at 32 kV/cm. Figure 6a also shows an example of the fluorescent microscope images for each tested EFT-Cu condition's LOAC cross-section. The images show the increase of fluorescence scattered across the board as the Cu concentration is increased, inactivating more cells on all positions on the LOAC surface, as well as the increase in intensity near the middle portion where the electric field strength is strongest. Although these results show similar trends to our previous paper focused on the synergy between EFT and Cu only, the impact of increasing the Cu concentration with the use of EFT is observed clearly here with only concentrations below the SMCL for drinking water (Jarin et al., 2024).

Figure 6b shows the inactivation percentage of EFT-Ag over a range of electric field strengths. The inactivation efficiency increases here for increasing Ag concentration and increased electric field strengths, similarly and as expected. Although for these low concentrations of Ag, there is not a significant difference observed for the varying concentrations as 100% inactivation is reached at 34 kV/cm when 30 μg/L is administered, but for the other cases 94% is reached using 20 μg/L, and 88% using 10 μg/L at the same maximum electric field strength of 34 kV/cm. Compared to the EFT-only condition with no added Ag, the EFT can reach 72% inactivation using a maximum 34 kV/cm, which is about 20%–30% lower than with any additional Ag. Figure 6b also shows an example of the fluorescent microscope images for each tested EFT-Ag condition's LOAC cross-section. The images show the increase of fluorescence scattered across the board as the Ag concentration is increased, similarly to Cu. Despite this, there is less fluorescence shown overall in comparison to the EFT-Cu as this is in line with the lower overall inactivation achieved from the calculated results. The impact of increasing the Ag concentration with the use of EFT is shown clearly here with concentrations below the SMCL, although there may not be a significant observable difference to the varying concentrations at this low level.

To analyze the potential synergy between EFT and each of these two metals, the S values were calculated for each case (Fig. 7). Generally, the positive S values indicate significant synergy between the EFT and metal ions, specifically as concentration and electric field strength increase. For EFT-Cu here, the 200 μg/L condition showed mostly additive behavior when combined with EFT, but for the 500 and 800 μg/L an increase in S values (increase in color intensity) was observed in the higher electric field strengths (28–33 kV/cm). Due to the wide set of data in the study, we believe the lower electric field strengths are more prone to showing some variance in their synergy values since the combined effects are not very different from the individual. Despite the variance, the range of negative values calculated in this study or in Fig. 7 are all still rather small in comparison to the positive synergy values we are more focused on in this work. The increase in S values here allows us to conclude the presence of synergy using EFT-Cu and its ability to increase with increasing electric field strength. Interesting to note, the color intensity declines a bit after peaking at 33–34 kV/cm. As the overall inactivation efficiency reaches 90%–100% (maximum capacity), the S values begin to decline as the inactivation can no longer increase. Because of this, the decline in S values near the highest electric field strengths are to be expected. Similar analysis is shown for the EFT-Ag. Specifically for EFT-Ag, we see positive S values mainly in the higher electric field strengths across all three concentrations tested. Despite this, there is no clear trend to the EFT-Ag synergy as the color intensity increase and decrease rather inconsistently for each concentration. Overall, the very prominent and positive S values confirm the presence of synergy between EFT and each antimicrobial metal while the electric field strength and concentration increases.

From the S values depicted in Fig. 7, there are two clear trends observed for the synergy between EFT and metals. Looking from the bottom to the top, there is a very clear increase in the synergy values as the electric field strength increases. The second trend is observed for EFT-Cu when looking from left to right as the synergy values generally increase as the concentration of metal ions also increases. Interestingly, Ag does not follow the same trend, as concentration does not seem to contribute to any specific peaks across the figure. We attribute this to the difficulty of experiment with Ag ion as it requires a much lower concentration to be within its SMCL. We admit this may be one limitation of our study, as we believe it is due to the closeness of the concentration range or the range being so little itself (< 0.1 mg/L) that makes the collected Ag data on the LOAC more widely varied than comparative Cu data.

The EFT-Cu peaks at 0.48 while EFT-Ag peaks at

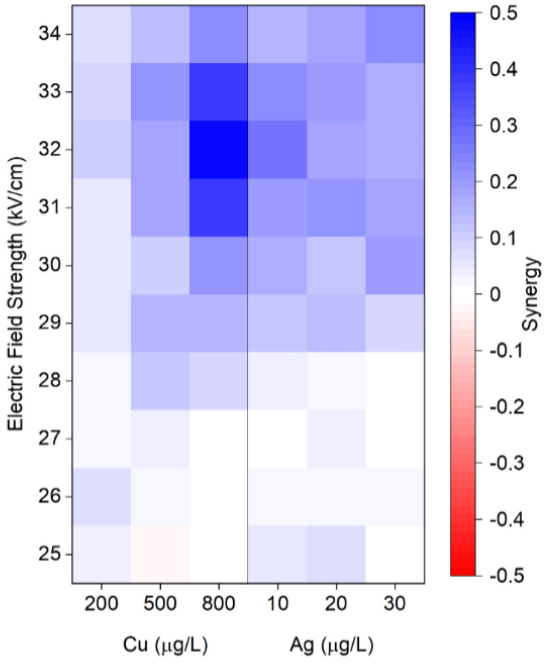

Fig. 7 Synergy (S) values determined via Bliss Independence Model for the combinations of EFT-Cu and EFT-Ag for varying electric field strengths (25–34 kV/cm). For color figure references, please consult the online version of this article.

0.28. This suggests Cu is a more effective and efficient synergistic metal ion to be used in combination with EFT as the highest S values are observed. As EFT-Cu has been studied previously, this high synergy observed is due to EFT is able to weaken the membranes of bacteria leaving them more susceptible to inactivation by Cu both internally and externally (Jarin et al., 2024). Similarly for EFT-Ag, a related study tested the removal/inactivation mechanism of *E. coli* with Ag ions and electric field, finding the main mechanism to be the increased cell membrane permeability caused by the externally applied electric field, enhancing the penetration of silver ions through biofilms/cells (Suttasattakrit et al., 2022). For our case, we believe the synergy potential may not be as significant here due to low concentrations of Ag used and the limited ability for Ag to contribute to further membrane damage or permeability increase after EFT has already successfully done so. Looking at the inactivation and S value results, there is great promise for the use of both EFT-Cu and EFT-Ag as they all had relatively high inactivation efficiency and positive S values for more than half of the analyzed cases.

3.4 Synergy when combining EFT with Cu and Ag

Understanding that Cu has potential synergies when combined with Ag, and that both metals have some synergy when combined with EFT, we tested the combination of EFT with Cu and Ag, and the results are shown in Fig. 8 in comparison to their respective individual results. We use three different concentrations cases with Case 1 (Fig. 8a) being the lowest concentrations combined, Case 2 (Fig. 8b) slightly increased concentrations, and Case 3 (Fig. 8c) being the highest. The data for the new combination of EFT with Cu and Ag (EFT-Cu-Ag) are specifically highlighted using the upright green triangles. Generally, we see higher overall inactivation for the EFT combination metal cases when compared to the individual EFT-Cu, EFT-Ag, and EFT-only cases. There is very clearly

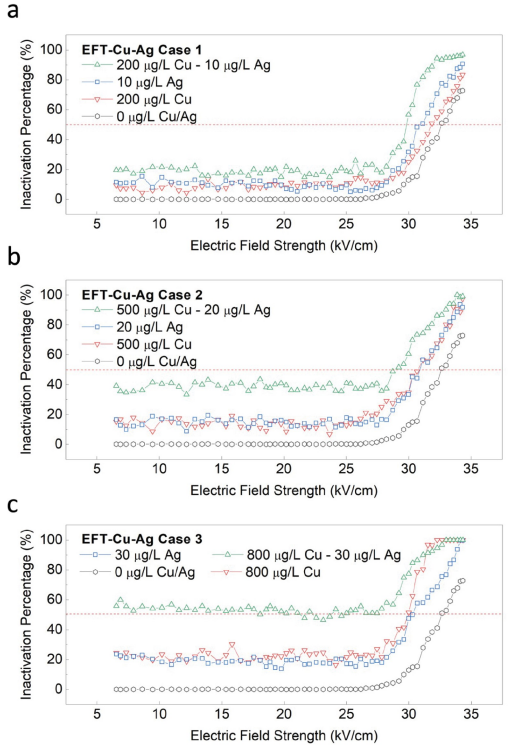

Fig. 8 Inactivation efficiency of EFT combined with Cu and Ag (EFT-Cu-Ag) for varying concentration cases observed on the LOAC. Three different concentrations cases are tested with Case 1 (a) being the lowest concentrations combined, Case 2 (b) slightly increased concentrations, and Case 3 (c) being the highest. The new EFT with Cu and Ag data are specifically highlighted using the upright green triangles. The same 70 V was applied to obtain a range of electric fields across the curved electrode from ~7–35 kV/cm. The red dashed line indicates the lethal electroporation threshold (LET), defined as 50% bacterial inactivation. Error bars reflecting 95% confidence intervals for each combined metal treatment group are presented in Fig. S3 in the SI. The red dashed line represents the lethal electroporation threshold (LET) where overall inactivation reaches 50%. For color-specific details, please refer to the web version of the article.

more inactivation achieved with lower electric field strength applied due to the increased presence of more antimicrobial metals in the combination cases. Additionally, for EFT-Cu-Ag Case 1 (Fig. 8a) where the lower concentrations are used in combination (green triangles), the largest difference in inactivation efficiency is seen when increasing electric field strength (compared to the independent cases shown in blue squares and red downward triangles). When using 34 kV/cm, Case 1 achieved ~97% inactivation, Case 2 achieved ~99%, and Case 3 achieved 100%. With the clear ability to successfully achieve > 97% inactivation for all cases, there is great promise in using combinations of antimicrobial metals with EFT at the device scale for a variety of applications including drinking water disinfection. We expect the synergy for EFT with Cu and Ag to be based on the same mechanisms of the individual metal ions inactivation and EFT combinations with the individual metals. Additionally, a two-way ANOVA was used to confirm the statistical significance in variance between the electric field strength and the difference in use of metals and metal combinations. Statistical significance was shown across the board in both the interaction with electric field strength and varying concentration cases ($p < 0.001$), meaning all tested variables (individual metal ions, electric field strength, and combination of metals) provided significantly different results and have significantly different impacts to our overall inactivation efficiency.

In Fig. 9, the BIM is shown side by side for EFT-Cu-Ag for each concentration case. The figure displays S values for all three concentration cases tested for 10 different electric field strengths. We observe mostly near zero values (−0.1–0.1) with lower electric field strengths (< 30 kV/cm), while strong positive (blue) values are observed above 30 kV/cm. Some antagonistic (red) values are observed, interestingly mainly isolated to the lower electric field strength and high concentration cases (lower right). Although some negative S values (< −0.2) are observed, we expect this with the wide variation of data obtained in these studies and with the high concentrations cases due to approaching the detection limits of our study. (Smith and Romesberg, 2007; Garza-Cervantes et al., 2017) Many positive S values are also observed with the highest being 0.43, among others when applying high electric field strength with the lowest concentrations. Interestingly, for the lowest concentration Case 1, Cu and Ag without EFT previously showed an S value of ~0.06 (from Fig. 5a), but here with the addition of EFT, the S value has increased greatly to 0.43 (from Fig. 9).

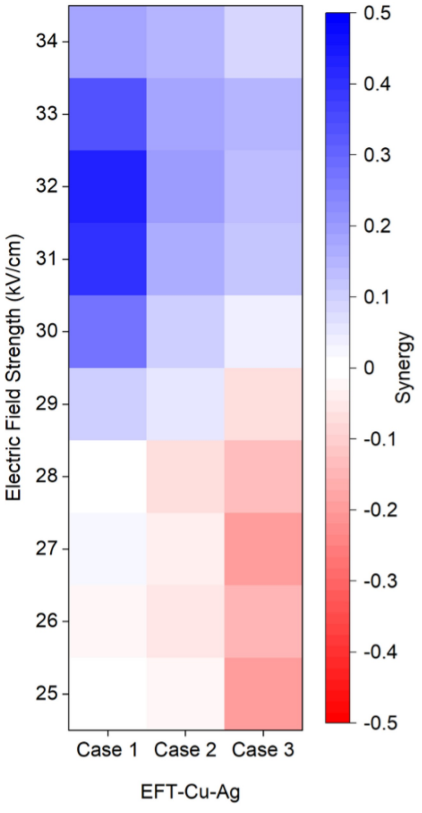

Fig. 9 Synergy (S) values determined via Bliss Independence Model for EFT combined with Cu and Ag for varying electric field strengths. The same 70 V was applied to obtain a range of electric fields across the curved electrode from ~7–35 kV/cm. For color figure references, please consult the online version of this article.

With these results using EFT with Cu and Ag, we believe some of the most promising synergies can be obtained when using EFT and antimicrobial metals at higher electric field strengths and lower concentration combinations. This is a very encouraging finding as we can optimize future approaches to take advantage of lower concentrations of metals in safe quantities while we tune the EFT in our favor. Regarding the S values, the highest S value when applying EFT (0.43 from Fig. 9) is higher than the S value for the highest concentration combination of Cu and Ag without any EFT (0.34 from Fig. 5a). The difference in these is that for the EFT with Cu and Ag, the highest synergy is observed with the lowest concentrations (Case 1 in Fig. 9) as opposed to the very limited synergy observed when the same concentrations are applied without any EFT (0.09 from Fig. 5a). Lastly, the high synergy values present in EFT combined with Cu and Ag (0.43 from Fig. 9) show immense promise for Cu and Ag to be studied further in combination with EFT at larger scale for its potential advantages in water treatment.

4 Discussion

The LOAC used in this study was developed specifically for experimenting and observing operando investigations under the microscope with EFT. Despite the many advantages of using an LOAC, there are still some limitations to address like the small sample size of bacteria immobilized on chip, inability to operate with a flow or mixed volume, and no successful way to transfer the cells in these experiments to a traditional plate count method to assess cell viability. (Jarin et al., 2024) Additionally, further work should focus on developing better methods to observe other bacteria species more consistently and especially chlorine resistant species using our lab-on-a-chip (LOAC) devices for future studies. Due to these limitation, further mechanism study of the EFT and antimicrobial metal attack pathways is not feasible and thus, future work can focus on redesigning the experiments in order to consider other analysis methods (electron microscopy, biochemical and membrane permeability assays, oxidative stress inhibitors, *etc*.) to more intensely investigate the mechanism of inactivation at the cellular level. Lastly, future work should also focus on testing wider ranges of metal concentrations, various other impactful parameters to pulse application in water treatment (pulse width, total effective treatment time, conductivity, pH, temperature, turbidity, *etc.*), and even different antimicrobial metals in combination with EFT (Garner, 2019). With all this considered, the strong consistency of results observed lead us to believe the synergies will be replicable at larger scales, in more realistic systems, for drinking water disinfection and pathogen prevention. On a larger scale, where increased concentrations of bacteria are used, the standard plate count method will be appropriate for analysis. For more details on larger scale studies focused on operation performance relevant to EFT in more complex water matrices, please refer to our previous works (Zhou et al., 2019, 2020; Mo et al., 2023). When applied in future at larger scales in batch, a variety of electric field strengths can not be tested all at once. Because of this, the results obtained in this study and the specific electric field strengths values found most optimal for synergy can be used to narrow the focus of future work to optimizing the applications at larger scale.

5 Concluding remarks

In this study, two antimicrobial metals (Cu and Ag) were tested using the LOAC device for both their synergies with one another and synergy when used in combination with EFT. Many strong synergies were confirmed and quantified between just the metals, but for this study, emphasis was placed on studying more specifically the synergy of EFT combined with Cu and/or Ag. The synergies were quantified using the Bliss Independent Model and possible mechanism involved in all combination cases were elucidated. Additionally, the strongest synergies were observed when combining EFT with Cu and Ag together at the microscale, showing great promise for future work focused on EFT-Cu-Ag at the application scale. Important to note, our tests conducted exhibit antibacterial effects at non-toxic concentrations for human cells and thus are still very promising for usage in drinking water disinfection. Therefore, in this work, we have concluded the promising synergy when combing EFT with Cu and Ag for potential applications in drinking water disinfection as the synergy was shown to be the strongest, while concentrations of both Cu and Ag remained well below the SMCL and safe for human consumption.

Conflicts of Interest Xing Xie is an Editorial Board Member of *ENGINEERING Environment*. The authors declare no known competing financial interests or personal relationships that could have influenced the work reported in this paper.

Acknowledgements The authors acknowledge funding support from the USA National Science Foundation (No. CBET 1845354). The authors also acknowledge Shruti Sarkar for their assistance in experimentation and Jacob Phaneuf for their support in statistical analysis. This work was performed in part at the Georgia Tech Institute for Matter and Systems, a member of the National Nanotechnology Coordinated Infrastructure (NNCI), which is supported by the USA National Science Foundation (No. ECCS-2025462).

Data Availability All data supporting the findings of this study are available within the article and its supplementary files. Any additional requests for information can be directed to, and will be fulfilled by, the corresponding authors.

Electronic Supplementary Material Supplementary material is available in the online version of this article at https://dx.doi.org/10.1007/s11783-026-2134-8 and is accessible for authorized users.

References

Alherek M, Basu O D (2023). Impact of low levels of silver, zinc and copper nanoparticles on bacterial removal and potential synergy in water treatment applications. Journal of Chemical Technology & Biotechnology, 98(5): 1137–1146

Alirezalu K, Munekata P E S, Parniakov O, Barba F J, Witt J, Toepfl S, Wiktor A, Lorenzo J M (2020). Pulsed electric field and mild heating for milk processing: a review on recent advances. Journal of the Science of Food and Agriculture, 100(1): 16–24

Araya M, Olivares M, Pizarro F, Llanos A, Figueroa G, Uauy R (2004). Community-based randomized double-blind study of gastrointestinal effects and copper exposure in drinking water. Environmental Health Perspectives, 112(10): 1068–1073

Arndt-Jovin D J, Jovin T M (1989). Fluorescence labeling and microscopy of DNA. Methods in Cell Biology, 30: 417–448

Benedict K M, Reses H, Vigar M, Roth D M, Roberts V A, Mattioli M, Cooley L A, Hilborn E D, Wade T J, Fullerton K E, et al. (2017). Surveillance for waterborne disease outbreaks associated with drinking water—United States, 2013–2014. MMWR Morbidity and Mortality Weekly Report, 66(44): 1216–1221

Berthelot P, Grattard F, Ros A, Lucht F, Pozzetto B (1998). Nosocomial legionellosis outbreak over a three-year period: investigation and control. Clinical Microbiology and Infection, 4(7): 385–391

Boukany P E, Morss A, Liao W C, Henslee B, Jung H, Zhang X L, Yu B, Wang X M, Wu Y, Li L, et al. (2011). Nanochannel electroporation delivers precise amounts of biomolecules into living cells. Nature Nanotechnology, 6(11): 747–754

Bragg P D, Rainnie D J (1974). The effect of silver ions on the respiratory chain of *Escherichia coli*. Canadian Journal of Microbiology, 20(6): 883–889

Carlson K M, Boczek L A, Chae S, Ryu H (2020). Legionellosis and recent advances in technologies for *Legionella* control in premise plumbing systems: a review. Water, 12(3): 676

CDC (2018). *Legionella* (Legionnaires' Disease and Pontiac Fever) Atlanta: U.S. Centers for Disease Control and Prevention

Dibrov P, Dzioba J, Gosink K K, Häse C C (2002). Chemiosmotic mechanism of antimicrobial activity of Ag^+ in *Vibrio cholerae*. Antimicrobial agents and Chemotherapy, 46(8): 2668–2670

Dietrich A M, Burlingame G A (2015). Critical review and rethinking of USEPA secondary standards for maintaining organoleptic quality of drinking water. Environmental Science & Technology, 49(2): 708–720

Dziewulski D M, Ingles E, Codru N, Strepelis J, Schoonmaker-Bopp D (2015). Use of copper-silver ionization for the control of legionellae in alkaline environments at health care facilities. American Journal of Infection Control, 43(9): 971–976

Feng Q L, Wu J, Chen G Q, Cui F Z, Kim T N, Kim J O (2000). A mechanistic study of the antibacterial effect of silver ions on *Escherichia coli* and *Staphylococcus aureus*. Journal of Biomedical Materials Research, 52(4): 662–668

Garner A L (2019). Pulsed electric field inactivation of microorganisms: from fundamental biophysics to synergistic treatments. Applied Microbiology and Biotechnology, 103(19): 7917–7929

Garrison L E, Kunz J M, Cooley L A, Moore M R, Lucas C, Schrag S, Sarisky J, Whitney C G (2016). Vital signs: deficiencies in environmental control identified in outbreaks of Legionnaires' disease—North America, 2000–2014. American Journal of Transplantation, 16(10): 3049–3058

Garza-Cervantes J A, Chávez-Reyes A, Castillo E C, García-Rivas G, Antonio Ortega-Rivera O, Salinas E, Ortiz-Martínez M, Gómez-Flores S L, Peña-Martínez J A, Pepi-Molina A, et al. (2017). Synergistic antimicrobial effects of silver/transition-metal combinatorial treatments. Scientific Reports, 7(1): 903

Gordon O, Vig Slenters T, Brunetto P S, Villaruz A E, Sturdevant D E, Otto M, Landmann R, Fromm K M (2010). Silver coordination polymers for prevention of implant infection: thiol interaction, impact on respiratory chain enzymes, and hydroxyl radical induction. Antimicrobial Agents and Chemotherapy, 54(10): 4208–4218

Grass G, Rensing C, Solioz M (2011). Metallic copper as an antimicrobial surface. Applied and Environmental Microbiology, 77(5): 1541–1547

Gupta V, Shekhawat S S, Kulshreshtha N M, Gupta A B (2022). A systematic review on chlorine tolerance among bacteria and standardization of their assessment protocol in wastewater. Water Science & Technology, 86(2): 261–291

Hegreness M, Shoresh N, Damian D, Hartl D, Kishony R (2008). Accelerated evolution of resistance in multidrug environments. Proceedings of the National Academy of Sciences of the United States of America, 105(37): 13977–13981

Helbling D E, Vanbriesen J M (2007). Free chlorine demand and cell survival of microbial suspensions. Water Research, 41(19): 4424–4434

Holt K B, Bard A J (2005). Interaction of silver(I) ions with the respiratory chain of *Escherichia coli*: an electrochemical and scanning electrochemical microscopy study of the antimicrobial mechanism of micromolar Ag^+. Biochemistry, 44(39): 13214–13223

Jarin M, Wang T, Xie X (2024). Operando investigation of the synergistic effect of electric field treatment and copper for bacteria inactivation. Nature Communications, 15(1): 1345

June S G, Dziewulski D M (2018). Copper and silver biocidal mechanisms, resistance strategies, and efficacy for *Legionella* control. Journal AWWA, 110(12): E13–E35

Jung W K, Koo H C, Kim K W, Shin S, Kim S H, Park Y H (2008). Antibacterial activity and mechanism of action of the silver ion in *Staphylococcus aureus* and *Escherichia coli*. Applied and Environmental Microbiology, 74(7): 2171–2178

LeChevallier M W (2019). Occurrence of culturable *Legionella pneumophila* in drinking water distribution systems. AWWA Water Science, 1(3): e1139

Lemire J A, Harrison J J, Turner R J (2013). Antimicrobial activity

of metals: mechanisms, molecular targets and applications. Nature Reviews Microbiology, 11(6): 371–384

Li J B, Lin H (2011). Numerical simulation of molecular uptake via electroporation. Bioelectrochemistry, 82(1): 10–21

Li W R, Xie X B, Shi Q S, Zeng H Y, Ou-Yang Y S, Chen Y B (2010). Antibacterial activity and mechanism of silver nanoparticles on *Escherichia coli*. Applied Microbiology and Biotechnology, 85(4): 1115–1122

Li W R, Xie X B, Shi Q S, Zeng H Y, Ou-Yang Y S, Chen Y B (2010). Antibacterial activity and mechanism of silver nanoparticles on *Escherichia coli*. Applied Microbiology and Biotechnology, 85(4): 1115–1122

Macomber L, Rensing C, Imlay J A (2007). Intracellular copper does not catalyze the formation of oxidative DNA damage in *Escherichia coli*. Journal of Bacteriology, 189(5): 1616–1626

Marambio-Jones C, Hoek E M V (2010). A review of the antibacterial effects of silver nanomaterials and potential implications for human health and the environment. Journal of Nanoparticle Research, 12(5): 1531–1551

Milani E A, Alkhafaji S, Silva F V M (2015). Pulsed electric field continuous pasteurization of different types of beers. Food Control, 50: 223–229

Mo F, Zhou J, Yu C, Liu F, Jumili M, Wu Y, Xie X (2023). Decoupling locally enhanced electric field treatment (LEEFT) intensity and copper release by applying asymmetric electric pulses for water disinfection. Water Research X, 21: 100206

Mouchtouri V, Velonakis E, Hadjichristodoulou C (2007). Thermal disinfection of hotels, hospitals, and athletic venues hot water distribution systems contaminated by *Legionella* species. American Journal of Infection Control, 35(9): 623–627

Pham A N, Xing G W, Miller C J, Waite T D (2013). Fenton-like copper redox chemistry revisited: Hydrogen peroxide and superoxide mediation of copper-catalyzed oxidant production. Journal of Catalysis, 301: 54–64

Prabhu B M, Ali S F, Murdock R C, Hussain S M, Srivatsan M (2010). Copper nanoparticles exert size and concentration dependent toxicity on somatosensory neurons of rat. Nanotoxicology, 4(2): 150–160

Raja F N S, Worthington T, Martin R A (2023). The antimicrobial efficacy of copper, cobalt, zinc and silver nanoparticles: alone and in combination. Biomedical Materials, 18(4): 045003

Raso J, Heinz V, Alvarez I, Toepfl S (2022). Pulsed Electric Fields Technology for the Food Industry. Cham: Springer

Ray P D, Huang B W, Tsuji Y (2012). Reactive oxygen species (ROS) homeostasis and redox regulation in cellular signaling. Cellular Signalling, 24(5): 981–990

Ricketts K D, Joseph C (2005). Legionnaires' disease in Europe 2003–2004. Eurosurveillance, 10(12): 11–12

Rohr U, Senger M, Selenka F, Turley R, Wilhelm M (1999). Four years of experience with silver-copper ionization for control of *Legionella* in a German university hospital hot water plumbing system. Clinical Infectious Diseases, 29(6): 1507–1511

Salah I, Parkin I P, Allan E (2021). Copper as an antimicrobial agent: Recent advances. RSC Advances, 11(30): 18179–18186

Smith P A, Romesberg F E (2007). Combating bacteria and drug resistance by inhibiting mechanisms of persistence and adaptation. Nature Chemical Biology, 3(9): 549–556

Soliman M Y M, Medema G, Van Halem D (2023). Enhanced virus inactivation by copper and silver ions in the presence of natural organic matter in water. Science of the Total Environment, 882: 163614

Suttasattakrit K, Khamkeaw A, Tangwongsan C, Pavasant P, Phisalaphong M (2022). Ionic silver and electrical treatment for susceptibility and disinfection of *Escherichia coli* biofilm-contaminated titanium surface. Molecules, 27(1): 180

Timmermans R A H, Mastwijk H C, Berendsen L B J M, Nederhoff A L, Matser A M, Van Boekel M A J S, Nierop Groot M N (2019). Moderate intensity Pulsed Electric Fields (PEF) as alternative mild preservation technology for fruit juice. International Journal of Food Microbiology, 298: 63–73

USEPA (1989). National primary drinking water regulations: filtration, disinfection, turbidity, giardia lamblia, viruses, legionella, and heterotrophic bacteria. Final Rule Fed Reg, 54(124): 27486

USEPA (2006). Ultraviolet Disinfection Guidance Manual for the Final Long Term 2 Enhanced Surface Water Treatment Rule. Washington: U.S. Environmental Protection Agency

USEPA (2024a). Secondary Drinking Water Standards: Guidance for Nuisance Chemicals. U.S. Environmental Protection Agency

USEPA (2024b). Stage 1 and Stage 2 Disinfectants and Disinfection Byproducts Rules. U.S. Environmental Protection Agency

USEPA (2024c). Technologies for Legionella Control in Premise Plumbing Systems. U.S. Environmental Protection Agency

Valko M, Morris H, Cronin M T D (2005). Metals, toxicity and oxidative stress. Current Medicinal Chemistry, 12(10): 1161–1208

Van Heijnsbergen E, Schalk J A C, Euser S M, Brandsema P S, Den Boer J W, De Roda Husman A M (2015). Confirmed and potential sources of *Legionella* reviewed. Environmental Science & Technology, 49(8): 4797–4815

Vasiliev G, Kubo A L, Vija H, Kahru A, Bondar D, Karpichev Y, Bondarenko O (2023). Synergistic antibacterial effect of copper and silver nanoparticles and their mechanism of action. Scientific Reports, 13(1): 9202

Wang T, Brown D K, Xie X (2022). Operando investigation of locally enhanced electric field treatment (LEEFT) harnessing lightning-rod effect for rapid bacteria inactivation. Nano Letters, 22(2): 860–867

Wang T, Chen H, Yu C L, Xie X (2019). Rapid determination of the electroporation threshold for bacteria inactivation using a lab-on-a-chip platform. Environment International, 132: 105040

Wang T, Xie X (2023). Nanosecond bacteria inactivation realized by locally enhanced electric field treatment. Nature Water, 1(1): 104–112

Wang T, Xie X (2024). Tuning the locally enhanced electric field treatment (LEEFT) between electrophysical and electrochemical

mechanisms for bacteria inactivation. Environmental Science & Technology, 58(33): 14875–14885

Warnes S L, Caves V, Keevil C W (2012). Mechanism of copper surface toxicity in *Escherichia coli* O157:H7 and *Salmonella* involves immediate membrane depolarization followed by slower rate of DNA destruction which differs from that observed for Gram‐positive bacteria. Environmental Microbiology, 14(7): 1730–1743

Warnes S L, Keevil C W (2011). Mechanism of copper surface toxicity in vancomycin-resistant enterococci following wet or dry surface contact. Applied and Environmental Microbiology, 77(17): 6049–6059

Weaver J C, Chizmadzhev Y A (1996). Theory of electroporation: a review. Bioelectrochemistry and Bioenergetics, 41(2): 135–160

Wen J J, Tan X J, Hu Y Y, Guo Q, Hong X S (2017). Filtration and electrochemical disinfection performance of PAN/PANI/AgNWs-CC composite nanofiber membrane. Environmental Science & Technology, 51(11): 6395–6403

Wright H, Gaithuma D, Heath M, Schulz C, Bogan T (2012). UV Disinfection Knowledge Base. Denver: Water Research Foundation

Xu Z W, Zhang C, Wang X, Liu D B (2021). Release strategies of silver ions from materials for bacterial killing. ACS Applied Bio Materials, 4(5): 3985–3999

Yang C D, Jiang L, Zhang H F, Shimoda L A, DeBerardinis R J, Semenza G L (2014). Analysis of hypoxia-induced metabolic reprogramming. Methods in Enzymology, 542: 425–455

Zhou J F, Wang T, Xie X (2019). Rationally designed tubular coaxial-electrode copper ionization cells (CECICs) harnessing non-uniform electric field for efficient water disinfection. Environment International, 128: 30–36

Zhou J, Wang T, Yu C, Xie X (2020). Locally enhanced electric field treatment (LEEFT) for water disinfection. Frontiers of Environmental Science & Engineering, 14(5): 78